Ceramics-Silikáty 66 (4), 447-452 (2022)
www.ceramics-silikaty.cz doi: 10.13168/cs.2022.0040

MESOPOROUS SULPHATE DOPED HYDROXYAPATITE NANOPARTICLES FOR CONTROLLED RELEASE OF PROTEINS

#AMMAR Z. ALSHEMARY*,**,***, YASSER MUHAMMED****, NADER A. SALMAN*****, ALI MOTAMENI******, RIZA GÜRBÜZ******

*Department of Chemistry, College of Science and Technology, Wenzhou-Kean University, Wenzhou, 325060, China
**Biomedical Engineering Department, Al-Mustaqbal University College, Hillah, Babil 51001, Iraq
***Biomedical Engineering Department, Faculty of Engineering, Karabuk University, Karabuk, 78050, Turkey
****Aeronautical Techniques Engineering, AL-Farahidi University, Baghdad, Iraq
*****Department of Medical Laboratory Techniques, Al-Manara College for Medical Sciences, Misan, 62001, Iraq
******Department of Metallurgical and Materials Engineering, Middle East Technical University, Ankara, 06800, Turkey

#E-mail: aalshema@kean.edu

Submitted July 27, 2022; accepted August 22, 2022

Keywords: Hydroxyapatite, Sulphate, Characterizations, Adsorption and desorption, Protein

The purpose of this study is to synthesize and characterize the mesoporous nanostructure of Hydroxyapatite (HA), evaluate the impact of the addition of sulphate ions (SO_4^{2-}) on the microstructure properties of HA, and assess the ability of the prepared materials to be used as a carrier for Bovine serum albumin (BSA) protein. This study successfully synthesized 0.07 mole of SO_4^{2-} substituted HA using the reflux microwave-assisted wet precipitation method and fully characterized it using modern techniques. In particular, XRD, XPS, Raman, FESEM, and BET techniques were used to explore the microstructure properties of materials. The results shows that the addition of SO_4^{2-} ions amplified the lattice parameters and surface area of HA, and the particles shape was changed from semi-spherical to rod like shape. Adsorption and desorption of protein molecules were evaluated using BSA protein for 24 h at 37 °C. BSA loading capacity and release behaviours were significantly improved with the incorporation of SO_4^{2-} ions. The SO_4- HA materials hold a promising future for being used as a carrier for protein molecules.

INTRODUCTION

Hydroxyapatite (HA) bears the excellent ability to be introduced into the mammalian body as a substitute material to repair various bone defects that may result either due to some injury or as a result of disease or infection. This broad use of HA, a popular bone material, is because of its similarity with the biological hard tissues [1]. Moreover, HA has been known for its outstanding applications in the biomedical field, particularly for orthopaedic surgery, due to its exceptional biocompatibility, osteoconductive, osteoinduction, bioactivity, and rapid osteointegration and similarity with the mineral phase of the mammalian bone system [2-4]. Owing to widespread applications of HA, numerous researchers are involved in accelerating their potential to upgrade the poor mechanical strength, wear strength, thermal stability, and biocompatibility [5].

HA can be synthesized in the laboratory using mineral-based chemicals. At the same time, it can also be synthesized using some biological resources, including bovine bone, fish bone, eggshells, and calcium or phosphate-based natural reserves [6-9]. Besides this, several researchers are also involved in doping some metals like Mg, Cu, Eu, etc. and some non-metal-based materials like OH^{1-}, SO_4^{2-}, F^{1-} etc. in the phase of pure HA to overcome the existing deficiencies of synthetic HA and tailor its properties according to the orthopedic surgeon's requirements.

According to previous studies, incorporating cations and anions may influence lattice parameters, crystallinity, crystal morphology, thermal stability, mechanical strength, and HA's ability to release some molecules. Each type of substitution has its own specific change. For instance, substituting Mg^{2+} ions may change HA lattice parameters and increase its dissolution rate. Similarly, anionic substitution may result in HA carrying various alternations in its structure and properties. Sulphate ions may replace phosphate ions present in the HA lattice and its incorporation enhances HA bioactivity and biocompatibility [10].

Sulphate ions (SO_4^{2-}) are the major sulphur source and the 4th most abundant molecule in human blood plasma. These ions are important and essentially required for cell growth, maintenance of the cell membrane, and and cell-matrix synthesis. Besides, these critical functions are equally needed to build and rebuild skin cells, nails, hair, and cartilage. These ions also provide protection to the cartilage cells against osteoarthritis.

In this investigation, sulphate doped HA was initially prepared using a wet precipitation method assisted by a reflux microwave system. During this work, the influence of the sulphate ion on the textural parameters was studied, and its effect on protein induction in the HA and finally its behaviour on the protein release ability was probed successfully. Results showed that sulphate substitution in the HA lattice shifts the parameters, broadening the HA peaks and exhibiting a reduction in the HA peak height, further affecting its bioactivity. In short, this study revealed that substituting sulphate ions in the HA lattice has a pronounced impact on HA structure, protein loading, and its release ability.

EXPERIMENTAL

All chemicals were purchased from Merck-Germany and were used without any further purification. Initially, HA and SO_4-HA materials were was synthesized using Calcium Nitrate [$Ca(NO_3)_24H_2O$ 1.0 M] and Di-ammonium hydrogen phosphate [$(NH_4)_2PO_4$ 6.0-XM], and sodium sulphate [Na_2SO_4 XM]. Both the solutions were prepared separately in doubly distilled water (DDW) and pH was maintained to 10 using ammonia solution. Then mixed both the solution slowly and shacked well for 15 min prior to heat inside the household microwave oven (800 W) equipped with a reflux condenser to furnish white suspension, which was later washed with DDW until pH became 7. The subsequent white suspension was dried in an oven at 80 °C for 17 h, and finally, white powder was heated in the muffled furnace at 1000 °C for 2 h so as to synthesize HA and SO_4-HA materials (Table 1).

Table 1. The nominal composition of the prepared materials.

Sample ID	Reactant (Mol)		
	Ca^{2+}	PO_4^{3-}	SO_4^{2-}
HA	1.00	0.60	0.00
SO_4-HA	1.00	0.53	0.07

X-ray diffraction (XRD, Rigaku Ultima IV) operated at 40 kV and 30 mA with CuKα radiation; a step size of 0.03/sec was inducted to probe the phase purity and crystallinity of the materials. All XRD spectras were recorded at 2 theta degree between 20 – 80°. PDXL (Ver.2.0) software (integrated X-ray powder diffraction software) was used to determine the sample's degree of crystallinity and lattice aparmters. Ramman shifts (Bruker FTRaman FRA/106S) were used to recognize the functionl groups using laser 785 nm. The X-ray phosphorous spectrometer (XPS, PHI 5000) spectra was inducted as a rapid quantitative tool to explore the chemical composition and Ca/P ratio of materials. Field emission scanning electron microscopy (FESEM, Quanta 400F) was introduced to explore the morphological structure of the materials. Specific surface area and pore size distribution studies of the materials were determined through Brunauer-Emmett-Teller (BET-Multiple Point, Quantachrome Corporation Autosorb 6) technique.

The adsorption and desorption assays were evaluated using Bovine Serum Albumin (BSA). To prepare 1 $mg{\cdot}mL^{-1}$ of BSA, about 300 mg of BSA was dissolved in 300 mL of Phosphate-buffered saline (PBS) and used as stock solution. Weighted powder samples (0.1 g) were immersed into 1.5 mL of 1 $mg{\cdot}mL^{-1}$ of BSA solution. After 24 h incubation time period, BSA solution was collected and analyzed to measure the adsorbed amount of BSA protein contents using a UV−Vis spectrophotometer. The incubation fluid was changed to PBS for the protein desorption investigation and protein desorption from powder samples was identified with a BCA test after a 24 h incubation period. Protein concentrations were calculated using a previously established calibration curve with known protein solution concentrations. Triplicates of the trials were carried out.

RESULTS AND DISCUSSION

XRD results have been displayed in Figure 1, which shows the appearance of sharp HA peaks and similarly shifting of the HA peaks after the doping of sulphate ions in the HA lattice. In the XRD spectra, sharp and well-developed HA peaks appear vivid and clear. XRD micrograph of the HA which shows Millar planes around (201), (002), (102), (211), (112), (300), (202), and (310) purely showing crystalline HA according to JCPDS card No. 09-432 (Figure 1 HA). Table 2 shows that the crystalline structure of HA had lattice parameters of a = b = 9.394 (Å) and c = 6.861(Å), a crystal size of about 22 nm, and a cell volume of about 524.39 $(Å)^3$. However, along with HA peaks, a tiny peak observed at 30.77° could be attributed to the diffraction plane (0210) belonging to β-Tricalcium Phosphate (βTCP, JCDPS No. 09-0169). The appearance of βTCP could be assigned to the decomposition of the HA phase at high temperatures formed in the reaction Equation 1:

$$Ca_{10}(PO_4)_6(OH)_2 \xrightarrow{1200\,°C/2h} 3Ca_3(PO_4)_2 + CaO + H_2O \qquad (1)$$

Considering the beneficial effects of βTCP, it is believed that its presence and HA will influence its resorption activity. It is well documented that the existence of βTCP improved the degradation rate of βTCP/HA composites. At the same time, the βTCP showed higher degradation compared to the HA structure [11].

Similarly, from the XRD pattern of SO_4-HA, it is quite evident that HA peaks are showing a slight shift towards the lower side on the 2-theta scale,

which is especially can be seen vibrantly around the Millar plane (002), (211), (112), (300) and (310). Besides this shifting, XRD peaks also demonstrated a broadening and shrinkage in the peak intensity. All these anomalies in the XRD peaks and lattice parameters could affect sulphate substitution in the HA structure. This shifting of the XRD peaks towards the lower side of the 2-theta angle, broadening of the peaks, and shrinkage of the peak intensity could be the result of successful doping of the bigger sulphate ion in the HA lattice. This increase in the cell dimension, decrease in the particle size, and reduction in the crystallinity of the HA structure could be ascribed to the substitution of large sized sulphate ions in the HA structure (Table 2) [12, 13].

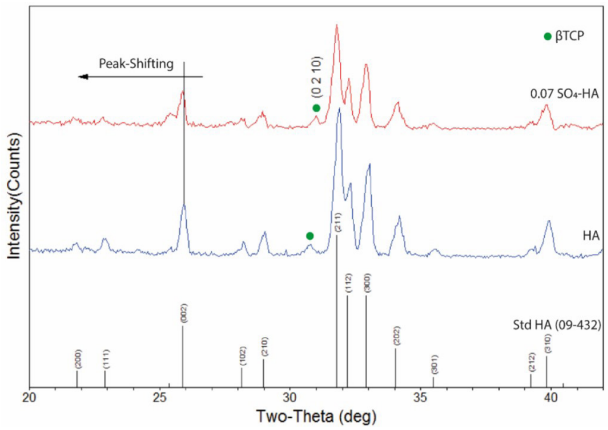

Figure 1. The XRD pattern of the HA and SO_4-HA presents the shifting of the XRD peaks after the doping of Sulphate ions.

Table 2. Displaying the Lattice parameters, crystallite size, and degree of crystallinity of pure HA and SO_4-HA.

Sample ID	Lattice Parameters			Crystallite size (nm)
	a-Axis (Å)	c-Axis (Å)	Cell Vol (Å)^3	
Std HA	9.418	6.884	528.8	-
HA	9.39408	6.86149	524.39	22
0.07 SO_4-HA	9.41257	6.8599	526.34	20

The Raman spectra of HA have been recorded in this study. It was observed that the Raman spectrum of the $(PO_4)^{3-}$(v1) band at 962 cm^{-1} was very intense and characteristic of HA. Specifically, it is linked to the fully symmetric stretching mode of the tetrahedral phosphate ion. The phosphate modes of 433 cm^{-1} $(PO_4)^{3-}$(v2), 589 cm^{-1} $(PO_4)^{3-}$(v4), and 1048 cm^{-1} $(PO_4)^{3-}$(v3) are observed. No significant change in the spectra location of the phosphate group was observed with the incorporation of SO_4^{2-} ions. Additionally, there was an overall increased intensity in the Raman spectra of pure HAs with the substitution of SO_4^{2-} ions. The strongest band of the S-O bond was located at 1017 cm^{-1}, which could be attributed to $(SO_4)^{2-}$(v1). Additional weak bands were observed at 675 cm^{-1} and 1129 cm^{-1}, which were assigned to the $(SO_4)^{2-}$(v4) and $(SO_4)^{2-}$(v3), respectively. The spectra band of $(SO_4)^{2-}$(v2) disappeared, which could be overlapped with the spectra of $(PO_4)^{3-}$(v2) at 433 cm^{-1}.

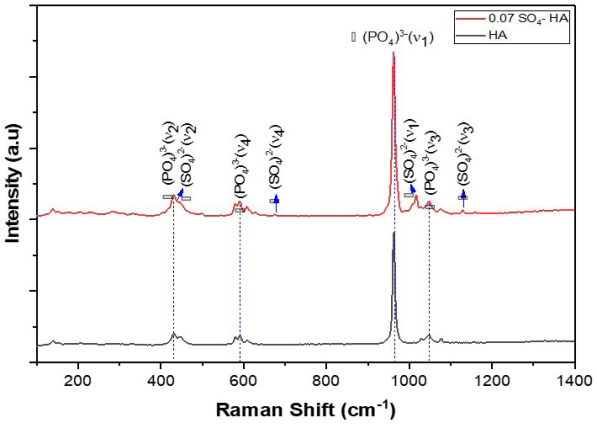

Figure 2. Raman Shift presents the impact of Sulphate doping on HA structure.

FESEM studies (Figure 3) revealed that poly-crystalline HA with a crystalline size of 22 nm had manifested a decrease in the particle size to 20 nm after doping a larger sulphate ion in the HA lattice. Similarly, the FESEM image (Figure 3b) reveals the development of rod-like morphology with sharp edges from polycrystalline morphology after successfully doping sulphate ions in the HA lattice.

XPS measurements describe the chemical compo/sition of the elements present on the surface of the HA and sulphate-doped HA (Figure 4). The spectras exhibit the presence of Ca (3p), Ca (3s), P (2p), P (2s), Ca (2p, 2p3), Ca (2s), and O (1s) located at 24, 43, 131, 190, 346, 438, and 528 eV, respectively. These peaks were indexed to the constituents of HA and are in good agreement with HA, as already filled in the literature. Similarly, XPS spectral studies in the case of SO_4-HA revealed that incorporating sulphate ions into the HA lattice has no significant shift in the binding energy of Ca and P. The S (2p) and S(2s) signals of sulphate group were recorded at 165 and 231 eV, respectively. Furthermore, the Na signal has also been detected at locations 498 and 1072 eV, which could be presented as a trace element during the washing process. The carbon signal at 282 eV might be due to carbon compounds adsorbed from the air, characteristic of apatite matrices [14]. The results further demonstrated that SO_4-HA contained the presence of sulphur, ensuring the successful doping of sulphate ions in the HA lattice.

The atomic Ca/P and Ca/P+S ratios have been measured using XPS analysis (Figure 4). The results showed that the Ca/P ratio of the pure HA and sulphate

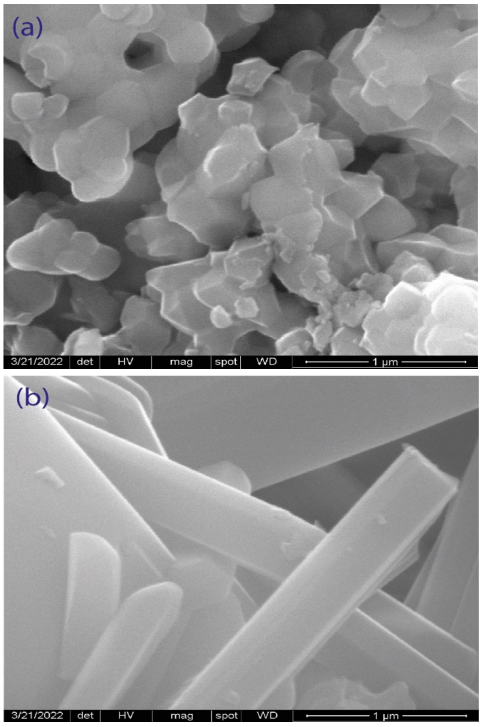

Figure 3. FESEM Image presenting the morphology of HA and SO_4-HA.

doped HA investigated in this study was lower than their stoichiometric ratio (1.67). This behaviour could be attributed to the loss of a small amount of minerals during the preparation and washing process. However, according to the literature, a Ca/P of less than 1.67 indicates the formation of highly calcium-deficient HA. The calcium-deficient HA benefits from a higher solubility, and consequently, it biologically appears more bioactive than HA [15]. The Ca/P ratio of pure HA was significantly reduced from 1.40 to 1.16 with the incorporation of sulphate ions, which could be attributed to incorporating some impurities such as Na ions into the Ca of HA. However, the presence of Na could be beneficial where it plays a vital role in various bone metabolic processes [16].

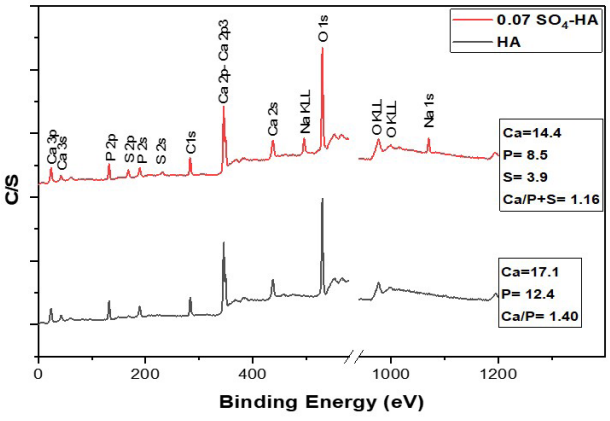

Figure 4. XPS study presenting the impact of Sulphate doping on HA structure.

The textural characteristics of the HA and SO_4-HA materials were investigated using N_2 adsorptiondesorption isotherms. Based on IUPAC classification, isotherms for all prepared materials are of type IV, and capillary condensation is accompanied by a narrow hemispherical meniscus (H3), indicating that all the samples have a mesoporous nature [17] (Figure 5). These mesopores are usually formed due to the clustering of primary crystallites [18].

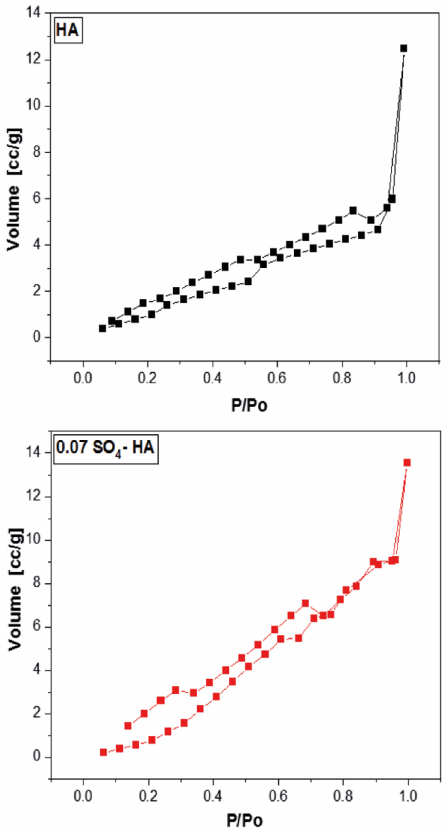

Figure 5. N_2 adsorption–desorption isotherm.

The amount of N_2 adsorbed was increased with the addition of SO_4^{2-} ions, indicating an expansion in pore size. Surface area, pore diameter, and pore volume measurements were carried out using the BET technique, and the results are summarized in Table 3. According to our studies, HA has displayed a surface area of around (5.379 $m^2 \cdot g^{-1}$), pore volume of around (0.0218 $cm^3 \cdot g^{-1}$), and a near pore size (22.46 Å). However, after the doping of sulphate ions in the HA lattice, an enhancement was noted in the three parameters. Results in the case of SO_4-HA exhibited a surface area of around (7.815 $m^2 \cdot g^{-1}$), pore volume of around (0.0264 $cm^3 \cdot g^{-1}$), and pore size of around (28.05 Å). This enhancement in the surface area, pore volume, and pore size could be attributed to the doping of large sulphate ions in the HA structure.

BSA protein adsorption studies on HA and SO_4-HA disc were studied at 37 °C for 24 h (Figure 6). Protein adoption study experiment confirmed that 0.72 $mg \cdot mL^{-1}$

was the final amount of BSA adsorbed (per HA disc) at the end of a 24h incubation period. However, after incorporating sulphate ion into the HA lattice, serum protein adsorption on SO_4-HA was increased up to 1.93 mg·mL^{-1}, which is significantly higher than the amount of serum protein adsorbed on the HA disc. This increase in loading capacity could be caused by electrostatic interactions or disulfide bonds between SO_4-HA and serum proteins, or it could be because SO_4-HA has a larger surface area than pure HA (Table 3).

Table 3. Textural parameters obtained by N_2 adsorption measurement.

Sample ID	Surface area ($m^2 \cdot g^{-1}$)	Pore V ($cm^3 \cdot g^{-1}$)	Pore Size (Å)
HA	5.379	0.0218	22.46
0.07 SO_4-HA	7.815	0.0264	28.05

Table 4. The adsorption and absorption behaviour after the doping of sulphate ions in the HA structure.

	HA	SO_4-HA
Adsorption Test	0.72 ± 0.19	0.13 ± 0.04
Desorption Test	1.94 ± 0.05	0.08 ± 0.01

On the other hand, the protein release behaviour test exhibited a reduction in the protein level in the case of SO4-HA (0.08 mg·mL^{-1}) in contrast to pure HA (0.13 mg·mL^{-1}). This reduction in case of protein release could be the effect of sulphate substitution in the HA lattice, which increases the binding sites in the HA struc-ture, reducing HA's release ability for proteins.

CONCLUSIONS

In this investigation, sulphate doped HA composite was synthesized using a wet chemical method assisted by a household microwave system linked with a reflux condenser. Our results revealed a successful substitution of sulphate ions in the HA structure. In light of various studies like XRD, XPS, Raman, FESEM, and BET, which have confirmed the successful doping of sulphate ions in the HA lattice, Furthermore, shifting of the XRD peaks towards the higher side of the 2-theta degree scale, Raman shift, and formation of rod-like morphology with sharp edges from polycrystalline morphology have confirmed that the size of the doped ions may influence the structure and morphology of the HA structure. High loading capacity of BSA with incorporation of sulphate ions into HA. SO_4-HA materials can be as a vehicle for protein molecules.

Acknowledgments

Dr. Ammar Z. Alshemary would like to thank Al-Mustaqbal University College. The authors would like to thank Dr. Muhammad Akram.

REFERENCES

1. Sharifianjazi, F., Esmaeilkhanian, A., Moradi, M., Pakseresht, A., Asl, M. S., Karimi-Maleh, H., Jang, H. W., Shokouhimehr, M., and Varma, R. S. (2021): Biocompatibility and mechanical properties of pigeon bone waste extracted natural nano-hydroxyapatite for bone tissue engineering. *Materials Science and Engineering: B, 264*, 114950. Doi:10.1016/j.mseb.2020.114950
2. Yelten-Yilmaz, A., and Yilmaz, S. (2018): Wet chemical precipitation synthesis of hydroxyapatite (HA) powders. *Ceramics International, 44*, 9703-9710. Doi:10.1016/j.ceramint.2018.02.201
3. He P., Sahoo S., Ng K. S., Chen K., Toh S. L., Goh J. C. H. (2013): Enhanced osteoinductivity and osteoconductivity through hydroxyapatite coating of silk-based tissue-engineered ligament scaffold. *Journal of biomedical materials research part A, 101*, 555-566. Doi:10.1002/jbm.a.34333
4. Cho J. S., Yoo D. S., Chung Y. C., Rhee S. H. (2014): Enhanced bioactivity and osteoconductivity of hydroxyapatite through chloride substitution. J*ournal of Biomedical Materials Research Part A, 102*, 455-469. Doi:10.1002/jbm.a.34722
5. Santhosh S., Prabu S. B. (2013): Thermal stability of nano hydroxyapatite synthesized from sea shells through wet chemical synthesis. *Materials Letters, 97*, 121-124. Doi:10.1016/j.matlet.2013.01.081
6. Akram M., Alshemary A. Z., Goh Y.-F., Ibrahim W. A. W., Lintang H. O., Hussain R. (2015): Continuous microwave flow synthesis of mesoporous hydroxyapatite. *Materials Science and Engineering: C, 56*, 356-362. Doi:10.1016/j.msec.2015.06.040
7. Akram M., Ahmed R., Shakir I., Ibrahim W. A. W., Hussain R. (2014): Extracting hydroxyapatite and its precursors from natural resources. *Journal of Materials Science, 49*, 1461-1475. Doi:10.1007/s10853-013-7864-x
8. Mohd Pu'ad N. A. S., Latif A. F. A., Ramli N. D., Muhamad M. S., Abdullah H. Z., Idris M. I., Lee T. C. (2020): Extraction of Biological Hydroxyapatite from Bovine Bone for Biomedical Applications. i*n Materials Science Forum, Trans Tech Publ, 1010*, 579-583. Doi:10.4028/www.scientific.net/MSF.1010.579
9. Malla K. P., Regmi S., Nepal A., Bhattarai S., Yadav R. J., Sakurai S., Adhikari R. (2020): Extraction and characterization of novel natural hydroxyapatite bioceramic by thermal decomposition of waste ostrich bone. *International journal of biomaterials, 2020*, 1690178. Doi:10.1155/2020/1690178
10. Alshemary A. Z., Pazarçeviren E. A., Dalgic A. D., Tezcaner A., Keskin D., Evis Z. (2019): Nanocrystalline Zn^{2+} and SO_4^{2-} binary doped fluorohydroxyapatite: A novel biomaterial with enhanced osteoconductive and osteoinconductive properties. *Materials Science and Engineering: C, 104*, 109884. Doi:10.1016/j.msec.2019.109884

11. Houmard M., Fu Q., Genet M., Saiz E., Tomsia A. P. (2013): On the structural, mechanical, and biodegradation properties of HA/β-TCP robocast scaffolds. *Journal of Biomedical Materials Research Part B: Applied Biomaterials, 101*, 1233-1242. Doi:10.1002/jbm.b.32935
12. Safarzadeh M., Ramesh S., Tan C. Y., Chandran H., Noor A. F. M., Krishnasamy S., Alengaram U. J. (2019): Effect of multi-ions doping on the properties of carbonated hydroxyapatite bioceramic. *Ceramics International, 45*, 3473-3477. Doi:10.1016/j.ceramint.2018.11.003
13. Ofudje E. A., Adeogun A. I., Idowu M. A., Kareem S. O. (2019): Synthesis and characterization of Zn-Doped hydroxyapatite: scaffold application, antibacterial and bioactivity studies. *Heliyon, 5*, e01716. Doi:10.1016/j.heliyon.2019.e01716
14. Sobierajska P., Nowak N., Rewak-Soroczynska J., Targonska S., Lewińska A., Grosman L., Wiglusz R. J. (2022): Investigation of topography effect on antibacterial properties and biocompatibility of nanohydroxyapatites activated with zinc and copper ions: In vitro study of colloids, hydrogel scaffolds and pellets. *Biomaterials Advances, 134*, 112547. Doi: 10.1016/j.msec.2021.112547
15. Beaufils S., Rouillon T., Millet P., Le Bideau J., Weiss P., Chopart J.-P., Daltin A.-L. (2019): Synthesis of calcium-deficient hydroxyapatite nanowires and nanotubes performed by template-assisted electrodeposition. *Materials Science and Engineering: C, 98*, 333-346. Doi:10.1016/j.msec.2018.12.071
16. Naqshbandi A., Rahman A. (2022): Sodium doped hydroxyapatite: Synthesis, characterization and zeta potential studies. *Materials Letters, 312*, 131698. Doi:10.1016/j.matlet.2022.131698
17. Motameni A., Dalgic A. D., Alshemary A. Z., Keskin D., Evis Z. (2020): Structural and Biological Analysis of Mesoporous Lanthanum Doped βTCP For Potential Use as Bone Graft Material. *Materials Today Communications, 23*, 101151. Doi: 10.1016/j.mtcomm.2020.101151
18. Popa C., Ciobanu C., Iconaru S., Stan M., Dinischiotu A., Negrila C., Motelica-Heino M., Guegan R., Predoi D. (2014): Systematic investigation and in vitro biocompatibility studies on mesoporous europium doped hydroxyapatite. *Open Chemistry, 12*, 1032-1046. Doi:10.2478/s11532-014-0554-y